

Homoclinic crossing in open systems: Chaos in periodically perturbed monopole plus quadrupolelike potentials

P.S. Letelier and A.E. Motter*

Departamento de Matemática Aplicada – IMECC,

Universidade Estadual de Campinas,

13081-970 Campinas, SP, Brazil

*[Phys. Rev. E **60**, 3920 (1999)]*

Abstract

The Melnikov method is applied to periodically perturbed open systems modeled by an inverse-square-law attraction center plus a quadrupolelike term. A compactification approach that regularizes periodic orbits at infinity is introduced. The (modified) Smale-Birkhoff homoclinic theorem is used to study transversal homoclinic intersections. A larger class of open systems with degenerated (nonhyperbolic) unstable periodic orbits after regularization is also briefly considered.

PACS numbers: 05.45.-a, 45.05.+x, 95.10.Ce

I. INTRODUCTION

Since the pioneering work of Poincaré [1] in celestial mechanics in which the mathematical basis of deterministic chaos in compact phase space systems was laid down, the study of homoclinic phenomena in closed systems with hyperbolic unstable periodic orbits has allowed the understanding of a rich variety of nonlinear effects in physics, chemistry, and biology [2]. Due to its universality, models in which unstable periodic orbits are subjected to small periodic perturbations has become one of the main paradigms of deterministic chaos [3]. An analytical tool to study such models is the Melnikov method [4, 5, 6] in connection with Smale-Birkhoff homoclinic theorem [7, 8], and Kolmogorov-Arnold-Moser (KAM) theory in the Hamiltonian case [9].

The Melnikov function describes the transversal distance between the stable and unstable manifolds associated to an unstable periodic orbit. Its isolated odd zeros indicate transversal intersections between these manifolds, and hence the onset of chaos [10]. Examples of applications of the Melnikov method in gravitation are the motion of particles in perturbed two- and three-dimensional Stäckel potentials [11, 12], the chaotic evolution of cosmological models [13], the study of orbits around a black hole perturbed by either gravitational radiation [14] or an external quadrupolar shell [15], and the bounded motion of particles in a periodically perturbed attractive center described by a monopole plus a quadrupolelike potential were considered in Ref. [16].

The Melnikov method has also been used in many other branches of physics. We find examples of applications of this method to the study of Josephson junctions [17, 18], planar periodic vortical flows [19], solitons [20], liquid crystals [21], and transfer dynamics of quasiparticles [22].

Even for Hamiltonian systems fundamental questions about chaos in non-compact phase space systems remain to be answered. Among the more important unsolved questions are the notion of chaos itself and the lack of an adequate theory to deal with it. Partial results obtained in this area are the fractal techniques in scattering processes [23], these are numerical techniques that present some difficulties due to the existence of different time scales for nearly bounded scattering. They are inadequate to the study of chaotic behavior arising from separatrices between bounded and unbounded orbits. Furthermore, they are unable to present a complete description of the chaotic motion as the one provided by analytical

methods in the closed system case.

The aim of this paper is to study the homoclinic phenomenon for a class of open systems that by a suitable change of coordinates can be approached in terms of an adequate formulation of the Melnikov method and Smale-Birkhoff homoclinic theorem. The change of coordinates regularizes the unstable periodic orbit at infinity and it compactifies the region of interest of the phase space; however, the phase space as a whole remains noncompact. Alas the resulting unstable periodic orbit is typically nonhyperbolic and the standard stable manifold theorem, needed to state the Melnikov method [10], does not apply. McGehee [24] extended this theorem to degenerated cases in the context of the Newtonian three body problem. Xia [25], and Dankowicz and Holmes [26], among others, used McGehee's result in connection with Melnikov method and Smale-Birkhoff homoclinic theorem to study the nonintegrability of the three body problem.

Here we consider the equatorial motion of a particle moving in a potential described by a monopolar term plus a quadrupolelike contribution. This potential models the gravitational attraction of a galaxy bulge or any nonspherical celestial body; it also arises in general relativity in the study of the motion of a test particle around a Schwarzschild black hole, the quadrupole term being a general relativistic effect associated to the angular momentum of the particle in the reduced two-dimensional phase space, see for instance Ref. [27].

In Sec. II the fixed saddle points associated to the monopole plus quadrupole system, as well as the coordinate transformation that regularizes these points at infinity, are studied. In the next section we present some mathematical preliminaries and the Melnikov method. The equations of motion are used to reduce this method to the analysis of simple graphics. We find that the perturbation induces transverse homoclinic orbits in some ranges of the parameters, and we apply the modified Smale-Birkhoff homoclinic theorem to verify the presence of a symbolic dynamics equivalent to a Smale horseshoe map; see Ref. [10]. In Sec. IV the study of the motion is completed with a presentation of Poincaré sections that reveal different levels of chaotic behavior as a function of the parameters. Finally, in the last section, we make some remarks about the class of system in which the same kind of analysis can be performed.

II. THE HOMOCLINIC ORBIT AND PERTURBATIONS

We shall consider the orbit of a particle in a plane under the influence of a force modeled by a potential with inverse square law plus a quadrupolelike term. It is convenient to work with dimensionless quantities. The motion of the particle is described by [16]

$$H_0 = \frac{p^2}{2} + \frac{1}{2r^2} - \frac{1}{r} - \frac{\beta}{r^3} \quad \left(p = \frac{dr}{dt} \right), \quad (1)$$

where r, p, t, H_0 , and β are dimensionless quantities proportional to, respectively, the radius, the radial momentum, the time, the Hamiltonian function, and the quadrupole moment of the attraction center. The effective potential

$$V_{eff} = \frac{1}{2r^2} - \frac{1}{r} - \frac{\beta}{r^3}, \quad (2)$$

is presented in Fig. 1 for different values of the parameter $\beta \geq 0$.

The natural space to study a periodically perturbed planar system is $\mathbb{R}^2 \times S^1$, where the unstable periodic orbits have a proper meaning [10]. In the corresponding unperturbed autonomous case the phase space is in \mathbb{R}^2 and the unstable periodic orbits reduce to fixed saddle points. The unstable periodic orbits are also reduced to fixed saddle points for the maps defined on Poincaré sections $\mathbb{R}^2 \times \{t_0\} \subset \mathbb{R}^2 \times S^1$.

The above system presents a homoclinic loop associated to the hyperbolic fixed saddle point at $(r, p) = (r_M, 0)$, where $1/r_M = 1/6\beta + \sqrt{(1/6\beta)^2 - 1/3\beta}$, for β limited by $1/16 < \beta < 1/12$. This case is important in the study of bounded orbits and was explored in Ref. [16].

In the present work we study the instabilities of unbounded orbits, the relevant values of the parameter are $\beta = 1/16$ and $0 \leq \beta < 1/16$. Let $H_0 = 0$, if $\beta = 1/16$ the points $r = r_M = 1/4$ and $r = \infty$ on the r axis represent fixed points such that the particle takes infinity time to reach to or to depart from each of these points. For zero energy still, if $0 \leq \beta < 1/16$ the motion of the particle is restricted to the region between $r = r_-$ and $r = \infty$, where $1/r_- = 1/4\beta - \sqrt{(1/4\beta)^2 - 1/\beta}$, and only the last point represents a fixed point in this range of values of β .

Since the orbits of interest are in a semi-infinity region bounded away from the origin, we can compactify this part of the phase space with a change of the position coordinate like $r = u^\alpha$ with $\alpha < 0$. We find that the transformation $r = 1/u^2$ allows us to model

the problem in a way similar to Refs. [24, 25, 26]. This new coordinate regularizes the fixed point at infinity that now is at the point $(u, p) = (0, 0)$. The zero energy orbits generate a heteroclinic loop for $\beta = 1/16$ associated to the hyperbolic fixed saddle point at $(u, p) = (2, 0)$ and the degenerated fixed saddle point at $(u, p) = (0, 0)$, and a homoclinic loop for $0 \leq \beta < 1/16$ associated to the degenerated fixed saddle point at $(u, p) = (0, 0)$. Degenerated in the sense that both eigenvalue of the linearized vector field are zero, as can be seen from the Hamiltonian equations

$$\frac{du}{dt} = -\frac{1}{2}u^3p, \quad (3)$$

$$\frac{dp}{dt} = -u^4 + u^6 - 3\beta u^8. \quad (4)$$

The points $(u, p) = (2, 0)$ and $(u, p) = (0, 0)$ correspond to, respectively, the hyperbolic fixed saddle point at $(r, p) = (1/4, 0)$ for $\beta = 1/16$ and the degenerated fixed saddle point at $(r, p) = (\infty, 0)$ for $0 \leq \beta \leq 1/16$. The homoclinic and heteroclinic loops are defined by the intersection between the stable and unstable manifolds on the (u, p) plane. The homoclinic loop for $\beta = 1/18$ is shown in Fig. 2 and the heteroclinic one is presented in Fig. 3.

The explicit integration of the homoclinic and heteroclinic loops will be necessary to apply the Melnikov method and can be obtained from the first integral of motion ($H_0 = 0$). For $\beta = 0$ we find

$$t(v) = \pm \frac{(1+v)(2-v)^{1/2}}{3v^{2/3}}, \quad (5)$$

where $v = 1/r$, the time origin is take in the symmetry point of loop, and the sign refers to the upper (+) and lower (-) parts of the loop. Analogously, for $0 < \beta < 1/16$ it reads

$$t(v) = \pm \sqrt{\frac{2}{\beta}} \left\{ \frac{(2v_+ + v_-)F(\delta, q) - 2(v_+ + v_-)E(\delta, q)}{3v_-^2 v_+^{3/2}} + \frac{v_+ v_- + (2v_+ + v_-)v}{3v_+ v_-^2} \sqrt{\frac{v_- - v}{(v_+ - v)v^3}} \right\} \quad (6)$$

with

$$\delta = \arcsin \sqrt{\frac{v_+(v_- - v)}{v_-(v_+ - v)}}, \quad q = \sqrt{\frac{v_-}{v_+}}, \quad (7)$$

where $F(\delta, q)$ and $E(\delta, q)$ are elliptic integrals of first and second type in the Legendre normal form (Ref. [28], p. 224), and $v_{\pm} = 1/4\beta \pm \sqrt{(1/4\beta)^2 - 1/\beta}$ are the roots of $V_{eff} = 0$.

Moreover, for $\beta = 1/16$ we get

$$t(v) = \pm \left\{ \frac{\sqrt{2}}{3} \left(\frac{1}{v^{3/2}} - \frac{1}{(4/3)^{3/2}} \right) + \frac{1}{2\sqrt{2}} \left(\frac{1}{\sqrt{v}} - \frac{1}{\sqrt{4/3}} \right) + \frac{1}{8\sqrt{2}} \ln \left[\left(\frac{2 - \sqrt{v}}{2 + \sqrt{v}} \right) \left(\frac{2 + \sqrt{4/3}}{2 - \sqrt{4/3}} \right) \right] \right\} \quad (8)$$

with the choice $t(4/3) = 0$, where $v = 4/3$ is the local minimum of V_{eff} .

Now, let us consider the Hamiltonian (1) perturbed by a periodic multipolar term of the form

$$H = H_0 + \varepsilon H_1, \quad (9)$$

$$H_1 = r^{-n} \cos(\Omega t) \quad (n \geq 2), \quad (10)$$

where $n = 2$ is dipolar, $n = 3$ is quadrupolar, etc. These perturbations can model the attraction due to a distribution of masses with periodic motions that are placed inside the planet orbit.

We shall consider our attraction center with a fix total mass. In other words, we excluded the monopolar case ($n = 1$) that represents a periodic variation of the mass.

In the next sections we study how these perturbations can affect the dynamics of the system.

III. MELNIKOV METHOD

Powerful tools to study near integrable systems are Melnikov type of techniques that detect transversal intersections between the stable and unstable manifolds associated to a unstable periodic orbit. The presence of such transversal intersections is a guarantee of complicated dynamics and in some cases leads to a symbolic dynamics equivalent to the Smale horseshoe [10].

In order to simplify the analysis it is convenient to abstract a little from the particular problem presented above. In what follows the loops are on the X plane and the manifolds are in the (X, θ) space, where $\theta \equiv t \bmod 2\pi/\Omega$ so that $(X, \theta) \in \mathbb{R}^2 \times S^1$, and Σ_{θ_0} denotes the section $\theta = \theta_0$. We consider a Hamiltonian of the form

$$\tilde{H}(X, t) = \tilde{H}_0(X) + \varepsilon \tilde{H}_1(X, t) \quad (\tilde{H}_1 \text{ } 2\pi/\Omega\text{-periodic in } t), \quad (11)$$

where \tilde{H}_0 is integrable with homoclinic (heteroclinic) loop Γ associated to some *hyperbolic* fixed saddle point(s). Under hyperbolicity hypothesis it can be shown that for sufficiently small ε the invariant manifolds are only deformed, and possibly their intersections become transversal, see for instance Ref. [10].

Let X_0 be a point on Γ and $X^{s/u}(\theta_0, \varepsilon)$ be points on the stable/unstable manifolds such that they are on Σ_{θ_0} , in the line perpendicular to $\Gamma \times \{\theta_0\}$ at X_0 and whose trajectories take the least amount of time to reach/depart any small neighborhood of the unstable periodic orbit. A computable measure of the transversal distance between the stable and unstable manifolds on Σ_{θ_0} , which defines the Melnikov function, is given by the zero order term of $1/\varepsilon[\tilde{H}_0(X^u(\theta_0, \varepsilon)) - \tilde{H}_0(X^s(\theta_0, \varepsilon))]$ [29]. In fact, if $X^{s/u}(t; \theta_0, \varepsilon)$ denotes the time evolution under \tilde{H} such that $X^{s/u}(\theta_0; \theta_0, \varepsilon) = X^{s/u}(\theta_0, \varepsilon)$, and $X_0(t)$ denotes the time evolution under \tilde{H}_0 such that $X_0(0) = X_0$,

$$\begin{aligned} \tilde{H}_0(X^{s/u}(\theta_0, \varepsilon)) - \tilde{H}_0(X^{s/u}(\pm\infty; \theta_0, \varepsilon)) &= \int_{\pm\infty}^{\theta_0} \frac{d\tilde{H}_0}{dt} [X^{s/u}(t; \theta_0, \varepsilon)] dt \\ &= \int_{\pm\infty}^{\theta_0} \frac{d\tilde{H}_0}{dt} [X_0(t - \theta_0), t] dt + O(\varepsilon^2). \end{aligned} \quad (12)$$

Thus in the homoclinic case the Melnikov function can be written as

$$M(\theta_0) = \frac{1}{\varepsilon} \int_{-\infty}^{\infty} \frac{d\tilde{H}_0}{dt} [X_0(t), t + \theta_0] dt, \quad \left(\frac{1}{\varepsilon} \frac{d\tilde{H}_0}{dt} = \{\tilde{H}_0, \tilde{H}_1\} \right), \quad (13)$$

where $\{ . , . \}$ are the usual Poisson brackets.

The implicit function theorem allows us to conclude that if $M(\theta_0)$ has simple zeros, then, for sufficiently small ε the invariant manifolds intersect transversely for some θ_0 . On the other hand, if $M(\theta_0)$ is bounded away from zero, then the invariant manifolds do not intersect for all θ_0 .

Now let us take the map defined by system (3)-(4) on a arbitrary section. After a scale change in the p coordinate it reads

$$u_{k+1} = u_k - C u_k^3 [p_k + O(4)], \quad (14)$$

$$p_{k+1} = p_k - C u_k^3 [u_k + O(3)], \quad (15)$$

where $C = \sqrt{2}\pi/\Omega$. Here the standard Melnikov method breaks down because of the degeneracy of the saddle point. McGehee [24], Xia [25], Dankowicz and Holmes [26] studied systems of this class in the context of the three body problem, where they established the

fundamental results needed to support the Melnikov method: structural stability of the unstable periodic orbits (trivial in our case since the degenerated unstable periodic orbit remains fixed); existence of local stable and unstable analytic manifolds C^∞ close to those of the unperturbed case [24, 26]; solutions on the perturbed and the unperturbed manifolds approach to the unstable periodic orbit at a similar rate [25, 26]. Following the proofs step-by-step we can observe that all the essential hypothesis involved to achieve their results are also satisfied by the above system. Thus these statements apply to Eqs. (14)-(15) allowing the expansion in Eq. (12) that justifies the use of Melnikov method in the present problem.

Another important result whose standard form assumes hyperbolicity is the Smale-Birkhoff homoclinic theorem. It was given a formulation of this theorem that is valid for the degenerated problem of Sitnikov [26], which is grounded on a suitable approximation of the linearization of the map in the neighborhood of the saddle point. Since such approximation results in the same expressions for the case of Eqs. (14)-(15), we conclude that the Smale-Birkhoff homoclinic theorem applies to the above system. Thus transversal homoclinic intersections in our problem lead to the Smale horseshoe.

Now we shall apply Melnikov method to Eq. (1) subjected to the perturbations (10). In the homoclinic case ($0 \leq \beta < 1/16$) we find for the Melnikov function

$$\begin{aligned} M(\theta_0) &= \int_{-\infty}^{+\infty} nr^{-n-1} \cos[\Omega(t + \theta_0)] \frac{dr}{dt} dt \\ &= -2n \sin(\Omega\theta_0) K(\Omega), \end{aligned} \quad (16)$$

$$K(\Omega) \equiv \int_0^{v^-} v^{n-1} \sin[\Omega t(v)] dv, \quad (17)$$

where we have fixed $X_0 = [v(0), p(0)]$ as the symmetry point on the loop and the integrand $t(v)$ means the positive branch of Eqs. (5)-(6). Thus the Melnikov function has simple zeros as long as $K(\Omega) \neq 0$. With the change $t \rightarrow v$ we pass from an infinite interval in Eq. (16) to a finite one in Eq. (17), and it allows us to study $K(\Omega)$ using graphics. Although u ($r = 1/u^2$) is important to justify the Melnikov method, we have great freedom in the choice of a coordinate to study the results. The most simple one that is adequate to this end is the coordinate $v = 1/r$.

The integrand of $K(\Omega)$ is formed by the product of an oscillating function and a polynomial. Near the origin this oscillation is a rapid one, since $t \rightarrow \infty$ as the particle goes to the unstable periodic orbit. In Fig. 4 we show a graph of $\sin[\Omega t(v)]$ for $\beta = 1/25$, and several values of Ω . For $\Omega > 4$ we will have more zeros in the interval shown in the figure. For $\Omega < 1$

the curve will look like the one for $\Omega = 1$. Since the area under the curves are clearly not null the integral of $\sin[\Omega t(v)]$ is nonzero for $\beta = 1/25$ and $0 < \Omega \leq 4$. The cases of interest are $n \geq 2$, where we will have a more favorable situation. We have transverse homoclinic orbits in all these cases. To better understand this behavior we show in Fig. 5 a graph of the integrand of $K(\Omega)$ for $\beta = 1/25$, $\Omega = 3$ and different values of n . For $0 \leq \beta < 1/16$ the graphics of $\sin[\Omega t(v)]$ will look like the one for $\beta = 1/25$, with almost the same upper bound for Ω . See for instance Fig. 6, where we plot the graphics of $\sin[\Omega t(v)]$ for the monopolar attraction center ($\beta = 0$) for the same values of Ω employed in Fig. 4. Therefore we have transverse homoclinic orbits for all β limited by $0 \leq \beta < 1/16$.

For these range of parameters the Smale-Birkhoff homoclinic theorem implies the existence of a hyperbolic invariant set for which the action of an N th iterate of the map has a symbolic dynamic equivalent to that of the Smale horseshoe map. Some important consequences of this result are sensitive dependence on initial condition (a characteristic of chaos); nonexistence of real analytic integral of motion (nonintegrable system); existence of infinitely many periodic orbits with arbitrary large periods (whose number increases exponentially with the period); capture of orbits by the system (in both directions of time).

It is illustrative to see how the chaotic orbits look in the original noncompactified coordinates r, p . Due to the lack of an extra integral of motion the particle can have a highly erratic motion and have access to a two dimensional region of the phase space. The sensitive dependence on initial condition implies that the evolution of two infinitesimally near points in the space r, p can result in two completely different bounded orbits, in two completely different unbounded orbits, or even in one bounded and one unbounded orbit. Orbits that are bounded for all $t < 0$ can go to infinite for $t \rightarrow +\infty$, and orbits of particles coming from infinite can remain bounded for all $t > 0$. However, regular orbits are also present and in particular there is a family of periodic orbits.

Let us consider the heteroclinic case $\beta = 1/16$. The Melnikov method obtained from Eq. (12) applies to each branch of the loop. The distance between $X^{s/u}(\pm\infty; \theta_0, \varepsilon)$ and $X^{s/u}(\pm\infty; \theta_0, 0)$ is of order $O(\varepsilon)$. Therefore $H_0(X^{s/u}(\pm\infty; \theta_0, \varepsilon))$ is of order $O(\varepsilon^2)$. Then, this term can be neglected and the Melnikov function reads

$$M(\theta_0) = 2n \sin(\Omega\theta_0)K_s(\Omega) - 2n \cos(\Omega\theta_0)K_c(\Omega), \quad (18)$$

$$K_s(\Omega) \equiv \int_0^{v^-} v^{n-1} \sin[\Omega t(v)] dv, \quad K_c(\Omega) \equiv \int_0^{v^-} v^{n-1} \cos[\Omega t(v)] dv. \quad (19)$$

The orbits in the heteroclinic loop are less symmetrical than in the homoclinic one and, consequently, the Melnikov function has simple zeros when at least one of the integrals of the previous formula is different from zero. The integrands of K_s and K_c oscillate very rapidly near the unstable periodic orbits. To better understand this behavior we show in Fig. 7 a graphic of the positive branch of Eq. (8). The function $t(v)$ has small values for a large range of values of v , and hence K_c will result nonzero values for small Ω . Indeed, we show in Fig. 8 a graph of $\cos[\Omega t(v)]$ for different values of Ω . Since cosine is an even function, the same figure is valid for the negative branch. For $\Omega > 3$ we will have more zeros in the interval $1 < v < 4$. For $\Omega < 0.5$ the curves will look like the one for $\Omega = 0.5$. For small values of n the integral K_c will be nonzero for $0 < \Omega \leq 3$. Due to the change of sign of $\cos[\Omega t(v)]$ near $v = 4$, the upper bound for Ω decrease with n . But it is clear from Fig. 8 that for each n will exist a upper bound $\Omega_o(n) > 0$ such that K_c will be nonzero, leading to the presence of transversal heteroclinic orbits, for $0 < \Omega \leq \Omega_o(n)$.

IV. POINCARÉ SECTIONS METHOD

The system (9) has four parameters, β , n , Ω , and ε . In opposition to the Melnikov method, Poincaré sections method is able to predict results only for fixed values of these parameters. However, the Poincaré method can locate the regular and irregular regions and provide a qualitative idea of chaotic behavior.

The perturbed phase space is in $\mathbb{R}^2 \times S^1$ and the maps defined on different values of the angular variable $\theta = t \bmod 2\pi/\Omega$ are topologically conjugated. So we have restricted the study to sections built on $\theta = 0$, but for a large number of different values of the parameters β , n , Ω , and ε . We included Ω values which would require a more elaborate numerical computation of the Melnikov function. In Fig. 9 we show the Poincaré sections for some select values of β , n , Ω , and ε . The general aspect of the sections is represented in this figure, with the predominance of irregular behavior near the destroyed invariant loop and the presence of a regular region near the center.

A careful analysis of the Poincaré sections reveals that chaos increases with n , which is natural since the major contribution of the perturbation comes from $v > 1$. In Figs. 9(a) and 9(b) we show the Poincaré sections for $n = 2$ and $n = 5$, respectively, where $\beta = 1/25$, $\Omega = 1$, and $\varepsilon = 0.003$. As a function of Ω , the most chaotic behavior occurs for frequencies

of the same order of the angular frequencies of the orbits in the local minimum of V_{eff} , from $(4/3)^2$ for $\beta = 1/16$ to 1 for $\beta = 0$. It is a reasonable result since for small Ω the system is almost autonomous, and for large frequencies the particle feels only an average of the multipolar motion that goes to zero for $\Omega \rightarrow \infty$. In Figs. 9(a), 9(c), and 9(d) we show Poincaré sections for $\Omega = 1$, $\Omega = 0.1$, and $\Omega = 5$, respectively, where $\beta = 1/25$, $n = 2$, and $\varepsilon = 0.003$. Also, the chaos increases strongly with the “size” of the perturbation ε . In Figs. 9(a) and 9(e) we show the Poincaré sections for $\varepsilon = 0.003$ and $\varepsilon = 0.01$, respectively, where $\beta = 1/25$, $n = 2$, and $\Omega = 1$.

The form of the orbits change with β , since there is a change in the destroyed loop, but the relative chaotic area of the section is almost independent of the value of β . In Figs. 9(a), 9(f), and 9(g) we show the Poincaré sections for $\beta = 1/25$, $\beta = 0$ and $\beta = 1/16$, respectively, where $n = 2$, $\Omega = 1$ and $\varepsilon = 0.003$. In particular, the case $\beta = 1/16$ presents two unstable periodic orbits and no higher chaotic behavior seems to be associated to it.

V. FINAL REMARKS

Making use of a compactification procedure and extensions of the standard Melnikov method and Smale-Birkhoff homoclinic theorem, we have detected transverse homoclinic and heteroclinic orbits and Smale horseshoe in periodically perturbed monopole + quadrupole-like potential. Moreover the compactified coordinates have proved useful to work out the Poincaré section method.

Although we have studied only one particular system, we stress that the approach is general and can be applied to a large class of open systems. The mathematical results depend essentially on the presence of the monopolar term in the unperturbed equations. Thus the same approach and with the same compactification applies to every inner-multipolar expansion model with nonzero monopolar contribution. In such cases we can allow non-Hamiltonian perturbations of the form $f(u, t, \varepsilon)$ in the equation corresponding to Eq. (4), where f is an analytic function of its variables, periodic in t , satisfying $f(u, t, 0) = 0$ and of order $O(u^6)$.

These systems represent very general situations. In the gravitational case, for instance, they can model a potential due to a mass distribution moving periodically with reflection symmetry. This includes all planar potential written as Fourier expansion in time together

with an inner-multipolar expansion in space variable. A specific example is provided by a Newtonian binary system perturbed by gravitational radiation. This system models the long-term dynamical evolution of binary systems of stars due to the emission and absorption of gravitational radiation [30].

In electromagnetic systems we can have a different situation. The possible absence of monopolar contribution creates a difficulty in transforming the map equations into the analytic form (14)-(15). The solution may be found using the Cassasayas-Fontich-Nunes's result, which establishes the Melnikov method for systems with parabolic degenerated saddle points [31]. A suitable compactification to treat the electromagnetic case is under study.

ACKNOWLEDGMENTS

The authors are thankful to CNPq and Fapesp for financial support.

[*] motter@ime.unicamp.br

- [1] H. Poincaré, *Les Méthodes Nouvelles de la Mécanique Celeste* (Gauthier-Villars, Paris, 1899), Vols. 1-3.
- [2] H. Bai-lin, *Chaos* (World Scientific, Singapore, 1982).
- [3] V.I. Arnold, *Dynamical Systems*, Encyclopaedia of Mathematical Sciences Vol. III (Springer-Verlag, Berlin, 1988).
- [4] H. Poincaré, *Acta Math.* 13 (1890) 1.
- [5] V.K. Melnikov, *Trans. Moscow Math. Soc.* 12 (1963) 1.
- [6] V.I. Arnold, *Sov. Math. Dokl.* 5 (1964) 581.
- [7] G.D. Birkhoff, *Dynamical Systems* (A.M.S. Publications, Providence, RI, 1927).
- [8] S. Smale, in: *Differential and Combinatorial Topology*, edited by S.S. Carins (Princeton University Press, Princeton, NJ, 1963), p. 63.
- [9] J. Moser, *Stable and Random Motions in Dynamical Systems* (Princeton University Press, Princeton, NJ, 1973) and references therein.
- [10] J. Guckenheimer and P. Holmes, *Nonlinear Oscillations, Dynamical Systems, and Bifurcations of Vector Fields* (Springer-Verlag, New York, 1983).
- [11] O.E. Gerhard, *Astron. Astrophys.* 151 (1985) 279.

- [12] O.E. Gerhard, *Mon. Not. R. Astron. Soc.* 222 (1986) 287.
- [13] J. Koiller, J.R.T. de Mello Neto, and I. Damião Soares, *Phys. Lett. A* 110 (1985) 260.
- [14] P.S. Letelier and W.M. Vieira, *Class. Quantum Grav.* 14 (1997) 1249.
- [15] R. Moeckel, *Commun. Math. Phys.* 150 (1992) 415.
- [16] P.S. Letelier and W.M. Vieira, *Phys. Lett. A* 242 (1998) 7.
- [17] X. Yao, J.Z. Wu, and C.S. Ting, *Phys. Rev. B* 42 (1990) 244.
- [18] A. Kenfack and T.C. Kofané, *Phys. Rev. B* 52 (1995) 10359.
- [19] T. Ahn and S. Kim, *Phys. Rev. E* 49 (1994) 2900.
- [20] F.Kh. Abdullaev, S.A. Darmanyán, and B.A. Umarov, *Phys. Rev. A* 41 (1990) 4498.
- [21] I.W. Stewart, T. Carlsson, and F.M. Leslie, *Phys. Rev. E* 49 (1994) 2130.
- [22] D. Hennig and B. Esser, *Phys. Rev. A* 46 (1992) 4559.
- [23] E. Ott, *Chaos in Dynamical Systems* (Cambridge University Press, Cambridge, 1994).
- [24] R. McGehee, *J. Diff. Eqns.* 14 (1973) 70.
- [25] Z. Xia, *J. Diff. Eqns.* 96 (1992) 170.
- [26] H. Dankowicz and P. Holmes, *J. Diff. Eqns.* 116 (1995) 468.
- [27] S. Chandrasekhar, *The Mathematical Theory of Black Holes* (Oxford University Press, Oxford, 1998)
- [28] I.S. Gradshteyn and I.M. Ryzhik, *Table of Integrals, Series, and Products*, 4th ed. (Academic Press, London, 1965).
- [29] A.M. Ozorio de Almeida, *Hamiltonian Systems: Chaos and Quantization* (Cambridge University Press, Cambridge, 1988).
- [30] C. Chicone, B. Mashhoon, and D.G. Retzlöff, *Class. Quantum Grav.* 14 (1997) 699.
- [31] J. Casasayas, E. Fontich, and A. Nunes, *Nonlinear Differ. Equ. Appl.* 4 (1997) 201.

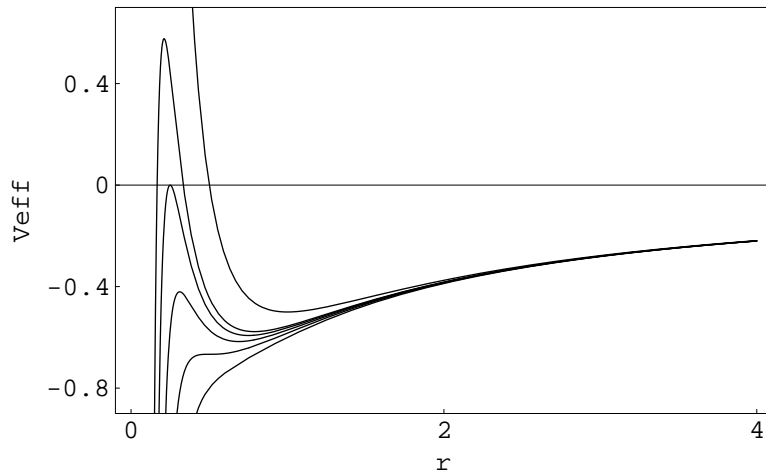


FIG. 1: The effective potential $[V_{eff}(r)]$ for $\beta = 1/10$ (bottom curve), $\beta = 1/12$, $\beta = 1/14$, $\beta = 1/16$, $\beta = 1/18$, and $\beta = 0$ (top curve), where the last one represents a monopolar potential.

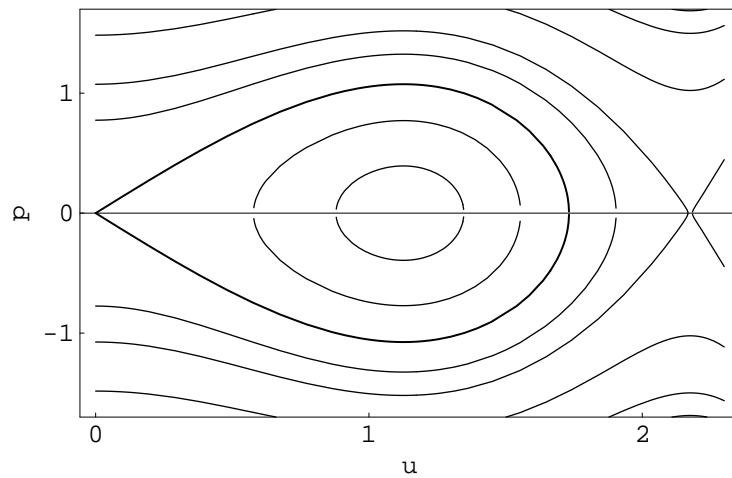


FIG. 2: The level curves of the Hamiltonian H_0 for $\beta = 1/18$. The homoclinic loop associated to $(u, p) = (0, 0)$ is the curve that contains that point.

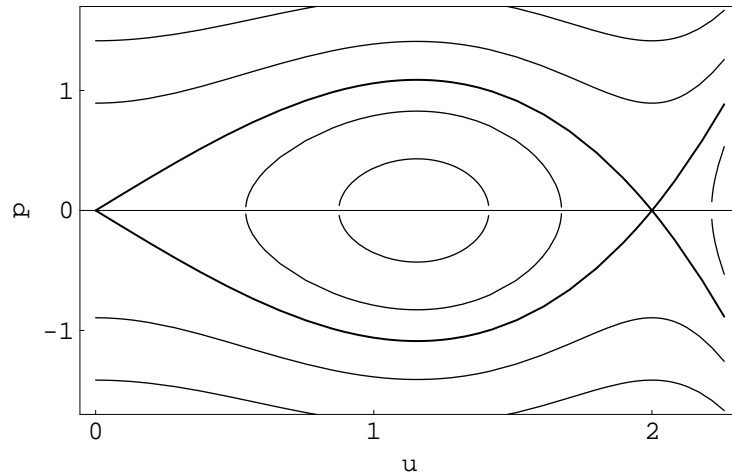


FIG. 3: The level curves of the Hamiltonian H_0 for $\beta = 1/16$. The curves that represent the invariant manifolds, which define the heteroclinic loop, associated to the points $(u, p) = (0, 0)$ and $(u, p) = (2, 0)$ are the curves that contains those points.

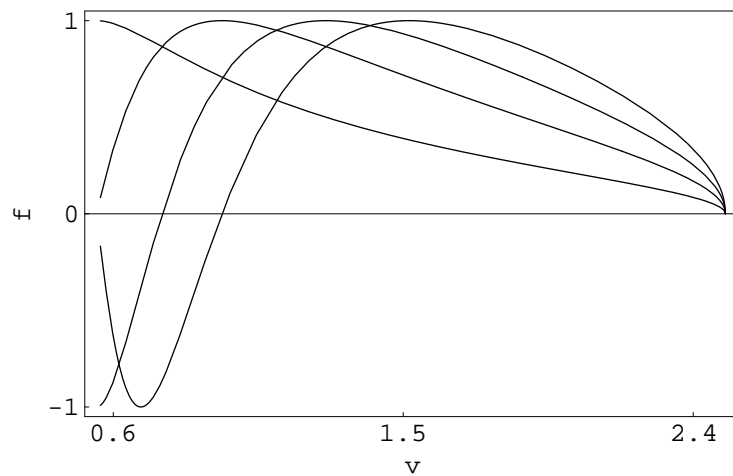


FIG. 4: $f \equiv \sin[\Omega t(v)]$ for $\beta = 1/25$, and $\Omega = 1$ (bottom curve), $\Omega = 2$, $\Omega = 3$, and $\Omega = 4$ (top curve).

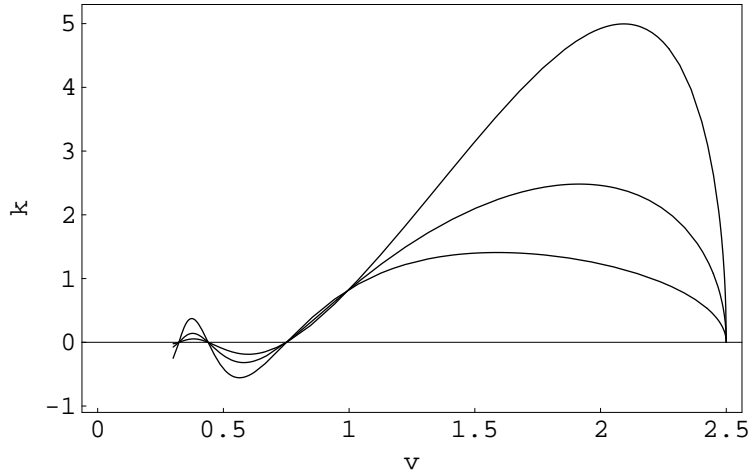


FIG. 5: The integrand $k \equiv v^{n-1} \sin[\Omega t(v)]$ of $K(\Omega)$ for $\beta = 1/25$, $\Omega = 3$, and $n = 2$ (bottom curve), $n = 3$ and $n = 4$ (top curve).

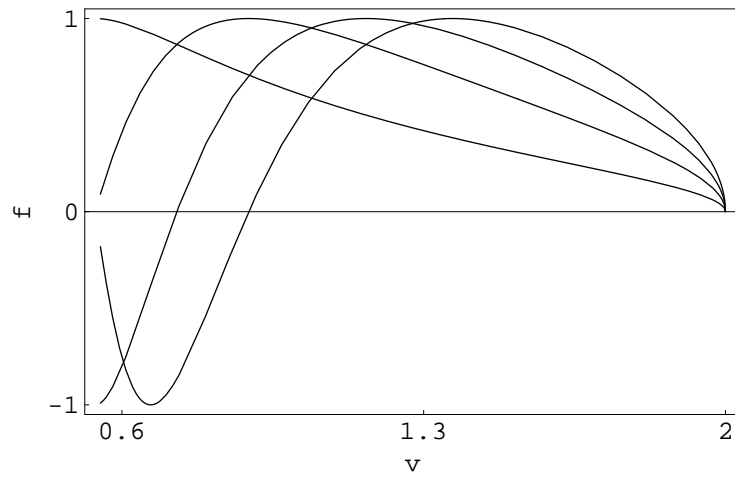


FIG. 6: $f \equiv \sin[\Omega t(v)]$ for the monopolar potential ($\beta = 0$) with $\Omega = 1$ (bottom curve), $\Omega = 2$, $\Omega = 3$, and $\Omega = 4$ (top curve).

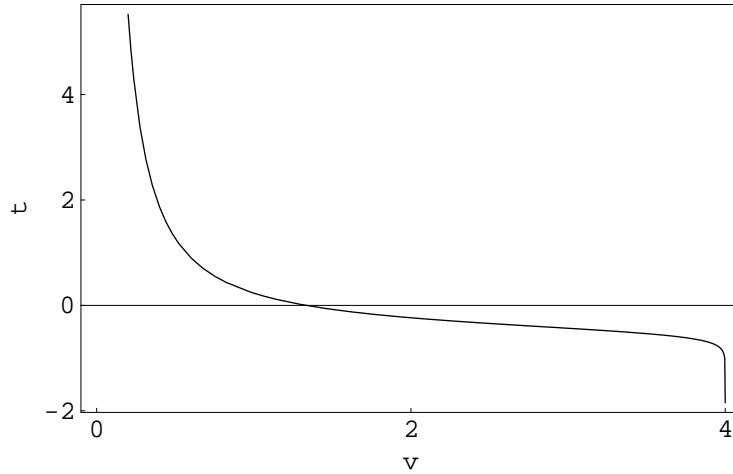


FIG. 7: The positive branch of Eq. (8): $t(v)$ goes to $\pm\infty$ at $v = 0$ and $v = 4$, but has small values at almost every point of the interval $0 < v < 4$.

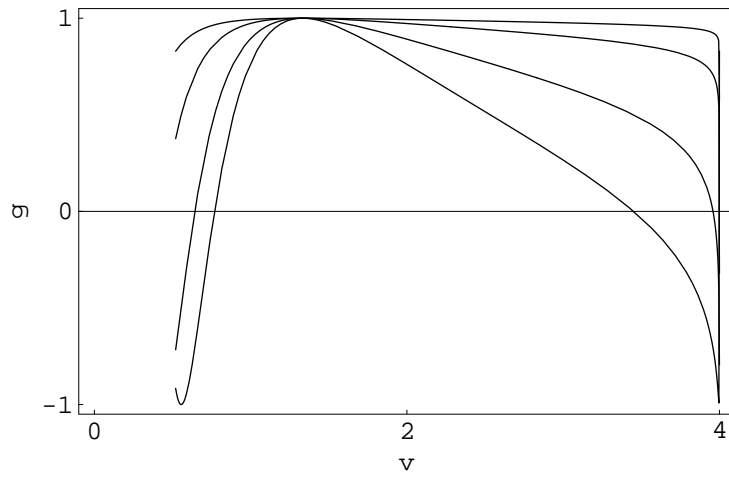


FIG. 8: $g \equiv \cos[\Omega t(v)]$ for $\beta = 1/16$, and $\Omega = 0.5$ (top curve), $\Omega = 1$, $\Omega = 2$, and $\Omega = 3$ (bottom curve).

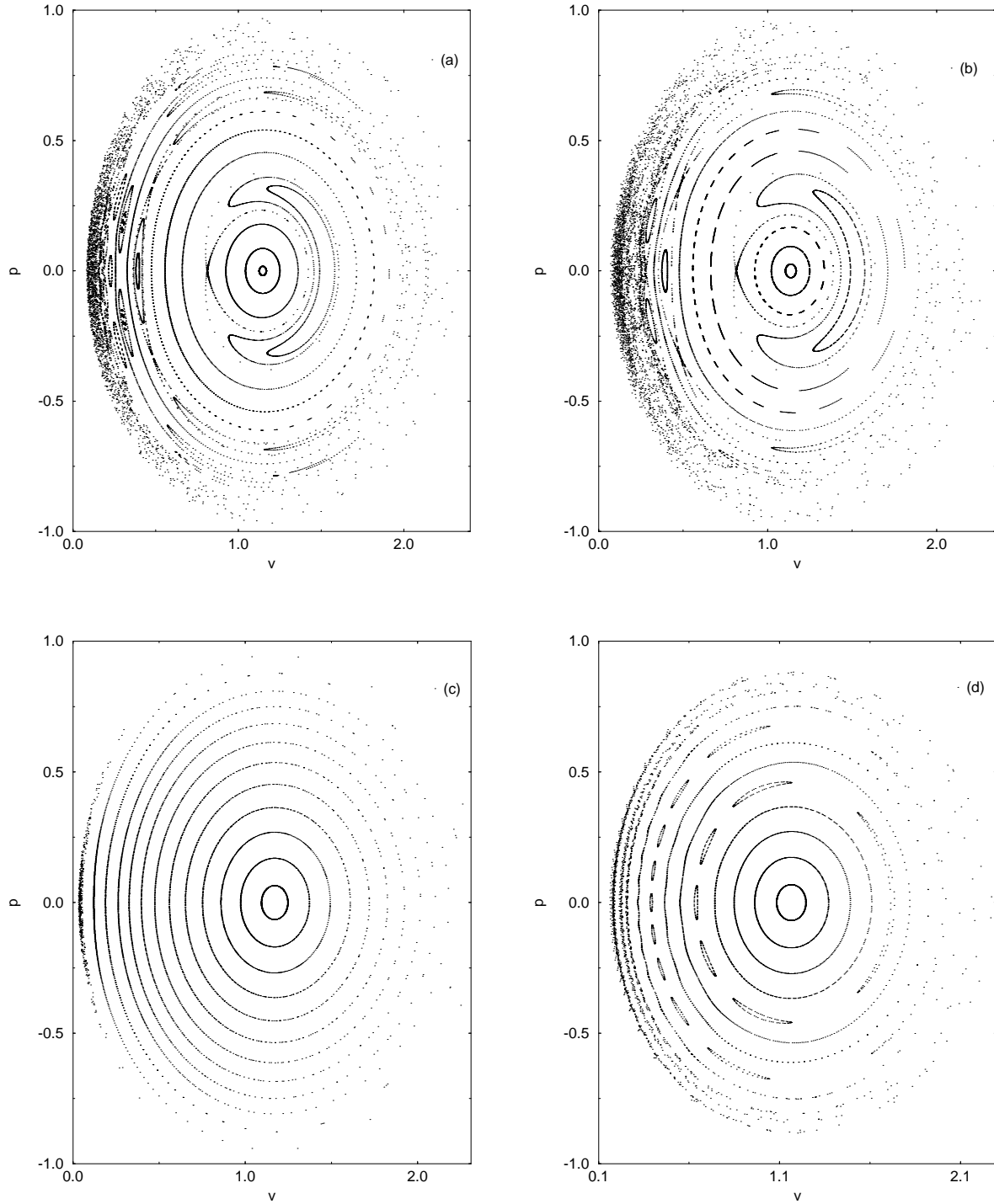


FIG. 9: The Poincaré sections for (a) $\beta = 1/25$, $n = 2$, $\Omega = 1$, and $\varepsilon = 0.003$; (b) $\beta = 1/25$, $n = 5$, $\Omega = 1$, and $\varepsilon = 0.003$; (c) $\beta = 1/25$, $n = 2$, $\Omega = 0.1$, and $\varepsilon = 0.003$; (d) $\beta = 1/25$, $n = 2$, $\Omega = 5$, and $\varepsilon = 0.003$; (e) $\beta = 1/25$, $n = 2$, $\Omega = 1$, and $\varepsilon = 0.01$; (f) $\beta = 0$, $n = 2$, $\Omega = 1$, and $\varepsilon = 0.003$; (g) $\beta = 1/16$, $n = 2$, $\Omega = 1$, and $\varepsilon = 0.003$.

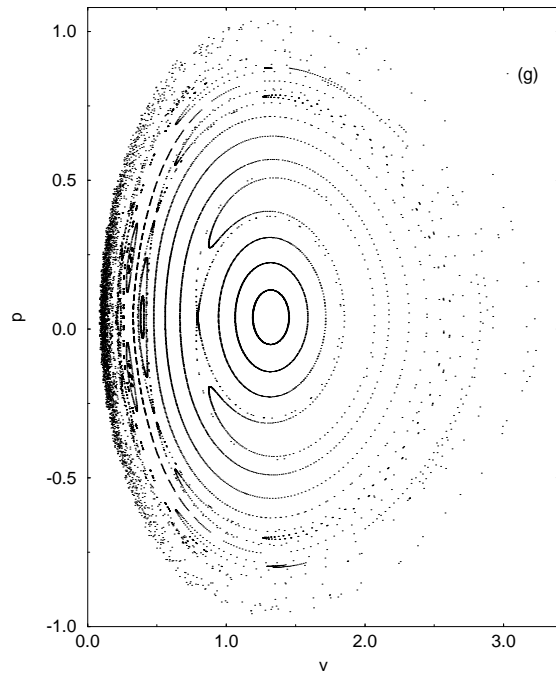
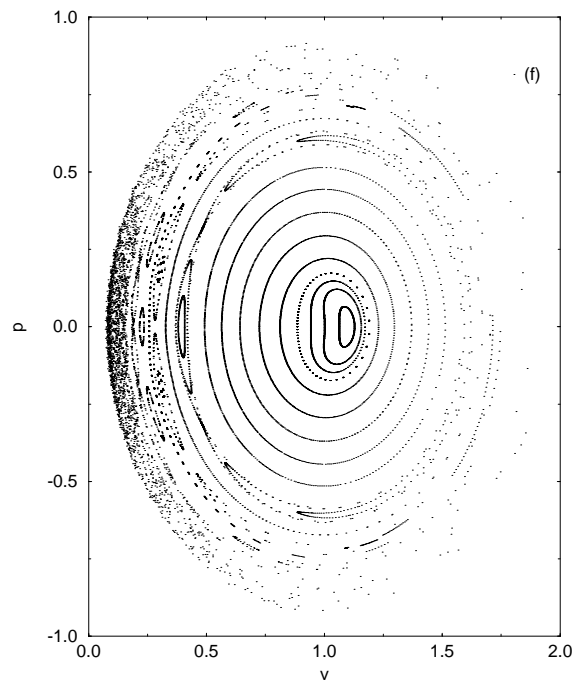
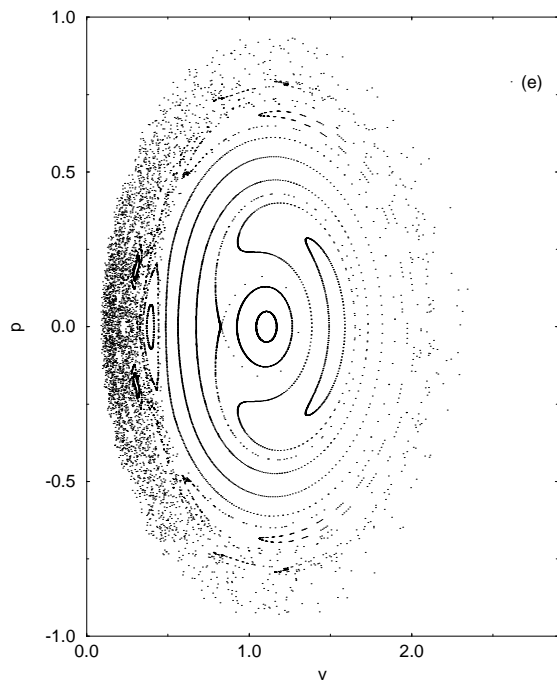


FIG. 9: (Continued)